NASA CR 66046

STUDY OF LOCAL FLOW CONDITIONS OVER A HEMISPHERICALLY BLUNTED 25° CONE FOR A SHALLOW RE-ENTRY TRAJECTORY

By

L. D. Wing and W. H. Eilertson

January 1966

Prepared under NASA-LRC Contract No. NAS1-5253--
Task II by
Martin Company--Baltimore Division
Baltimore, Md. 21203

for

NATIONAL AERONAUTICS AND SPACE ADMINISTRATION

CONTENTS

ILLUSTRATIONS

STUDY OF LOCAL FLOW CONDITIONS OVER A HEMISPHERICALLY BLUNTED CONE FOR A SHALLOW RE-ENTRY TRAJECTORY

By L. D. Wing and W. H. Eilertson
Martin Company, Baltimore Division

33979

SUMMARY

A study has been made of the aerodynamic heating, wall shear stress and local flow field properties for a 25 degree half-angle conical vehicle with a 3 in. (7.62 cm) spherically blunted nose and a 30 in. (76.2 cm) diameter base entering the atmosphere in a zero-lift re-entry trajectory. The initial conditions of re-entry are: relative flight path angle of -4.29 degrees; relative velocity of 26,000 fps (7.925 km/s) and initial altitude of 433,200 ft (132 km). A trajectory is presented for these re-entry conditions with the vehicle angle of attack constant at zero degrees. In addition, the laminar and turbulent heat rate and wall shear stress histories, the local (external to the boundary layer) histories of density, temperature, enthalpy, pressure, viscosity, Mach number and Reynolds number (based on local properties and surface distance from the stagnation point) are presented for body stations: s/R_N (surface distance from stagnation point non-dimensionalized with nose radius) = 1.0, 2.25, 3.0, 4.0, 5.0 and 10.0.

INTRODUCTION

The work presented in this volume responds to Phase 4 of Task II (NAS 1-5253-2) as defined in the work statement. This phase consists of the calculations of a re-entry trajectory for an axisymmetric (blunted cone) vehicle (see Fig. 1) at 0° angle of attack with initiating re-entry conditions specified. The vehicle consists of a 25° half-angle cone with a 3 inch (7.62 cm) spherically blunted nose and a 30 in. (76.2 cm) diameter base. In addition, pressures, heat transfer rates, shear stresses at the wall and local flow field properties (ρ_e, μ_e, M_e, i_e, T_e, p_e, and Re_s) are defined. A smooth body in equilibrium air is a specified assumption in the analysis. The 1959 ARDC atmosphere is used throughout and all calculations are based on T_w = 540° R (300° K).

The theoretical methods used in the analysis of the axisymmetric vehicle are identical to those used in the HL-10 analysis (see Sect. IV-A, Ref. 1) and are described in the heat rate section of this report. The applicability of the assumption of axisymmetry, however, is completely valid for the axisymmetric vehicle since the angle of attack is zero. Note that the local values of density, viscosity, Mach number, temperature and enthalpy refer to the local conditions just outside of the boundary layer. The pressure is, of course, assumed constant across the boundary layer. The local Reynolds number is based upon the local (external to boundary layer) density, viscosity and velocity combined with the surface distance from the stagnation point.

The NASA technical representative for all work described in this report was Mr. C. Pittman of the Structures Research Division,and the technical monitors were Messrs. J. L. Raper and R. L. Wright of the Applied Materials and Physics Division at Langley Research Center, Hampton Va.

SYMBOLS

A	=	Area
B	=	Constant = 1.12
C_D	=	Drag coefficient
C_f	=	Friction coefficient
C_p	=	Specific heat at constant pressure (Btu/lbm °R or J/kg °K)
$\overline{C}_f$	=	Average skin friction coefficient
g	=	Acceleration of gravity (sea level) (ft/sec^2 or Nm^2/kg^2)
h	=	Altitude, ft (km)

H_s^* and H_0^* are defined by Eqs. 15 and 16

i	=	Enthalpy (Btu/lbm or J/kg)
k	=	Thermal conductivity (Btu/ft sec °R or J/ms °K)
K	=	Term defined in Eq. 7
ℓ	=	Cone length (ft or m)
m	=	Mass (lbm or kg)
M	=	Mach number
N	=	Resultant load factor (g or kg/m^2)
p	=	Pressure (lbf/ft^2 or N/m^2)
Pr	=	Prandtl Number
$\dot{q}$	=	Heat transfer rate (Btu/ft^2 sec or watts/m^2)
$\overline{q}$	=	Dynamic pressure (lbf/ft^2 or N/m^2)
Q	=	Stagnation point total heat (Btu/ft^2 or J/m^2)

r	=	Normal distance from free-stream velocity vector (extended aftward from stagnation point) to body surface at appropriate s station (equals unity for 2 dimensional flow) (becomes local radius for cone) (ft or m)
r_B	=	Radius of cone base (ft or m)
$\bar{r}$	=	Recovery factor
R	=	Range (n. mi. or Mm)
Re_ℓ	=	Reynolds Number based on total vehicle length and free-stream flow properties
Re_s	=	Reynolds Number based on s distance and local flow properties (see Eq. 23)
R_N	=	Nose radius (ft or m)
s	=	Streamline or surface distance from stagnation point (ft or m)
T	=	Temperature (°R or °K)
V	=	Velocity (ft/sec or m/s)
Z	=	A counter: 0 for two dimensional flow, 1 for axisymmetric flow } see Eqs. 15, 16 and 22
α	=	Angle of attack (deg)
γ	=	Flight path angle (deg)
$\bar{\gamma}$	=	Specific heat ratio
θ	=	Cone half-angle
μ	=	Viscosity (lbf sec/ ft^2 or N s/m^2)
ρ	=	Density (slugs/ft^3 or kg/m^3)
τ	=	Shear stress at wall (lbf/ft^2 or N/m^2)
ψ	=	Heading angle (between velocity vector and vehicle centerline in horizontal plane) (deg)

Subscripts

B	=	refers to cone base
c	=	cone surface
e	=	evaluated at edge of boundary layer
f	=	due to friction
ℓ	=	vehicle length
rec	=	evaluated at boundary layer recovery enthalpy and local pressure
ref	=	vehicle reference value
R	=	relative to local earth horizontal
s	=	at surface distance from stagnation point
turb	=	turbulent boundary layer
w	=	evaluated at wall conditions
ZL	=	at zero lift
∞	=	free stream value
0	=	at stagnation point
2	=	conditions behind oblique shock

TRAJECTORY

The UB088 digital program of Ref. 2 was used to generate the axisymmetric vehicle re-entry trajectory. This is an n-phase atmospheric trajectory program capable of generating point mass trajectories traversing three-dimensional paths about an oblate rotating planet. A fourth order Runge-Kutta integrating procedure was used with variable computing interval to control the relative error. Aerodynamic data was input as a function of M_∞ and $M_\infty^{0.618}/\sqrt{Re_\ell}$. The 1959 ARDC atmosphere was used. Interpolation of input functions was first order. Relative initial conditions of V_R, γ_R and ψ_R were input along with geodetic coordinates to define initial positions. The program is written in FORTRAN II, incorporating an executive arrangement of subroutines.

The initial conditions for the axisymmetric re-entry trajectory specified in the work statement are:

γ_R = -4.29° (relative flight path angle)

V_R = 26,000 fps (7.925 km/s) (relative velocity)

h = 433,200 ft (132 km) (altitude)

$m/C_D A_{ref}$ = 100 lbm/ft^2 (488.24 kg/m^2)

Latitude = 28.25°

Longitude = -62.90°

Heading angle, 136°, clockwise from North

Angle of attack, α = 0°

The vehicle mass was calculated using the hypersonic value for drag (see Fig. 2) and the base area of the cone (4.92 ft^2 = 0.457 m^2). This results in a mass of 197 lb (89.3 kg). $C_D A$ was varied with Mach number as indicated in Fig. 2.

Axisymmetric Configuration Aerodynamics

The axisymmetric configuration aerodynamics consist of drag data only, since the vehicle is at 0° angle of attack. Inviscid aerodynamic drag was estimated using Refs. 3 through 6. The forebody drag was estimated using Ref. 3 for the subsonic value. At $M_\infty = 0.6$, $C_D = 0.080$ (pp 16-18, Fig. 23 of Ref. 3). At $M_\infty = 1.0$, $C_D = 0.44$ using Fig. 24, pages 16 to 18 of Ref. 3. Above M_∞ = 1.0 the following equation from pages 16 to 20 of Ref. 3 was used

$$C_D = 2.1 \sin^2 \theta_c + \frac{0.5 \sin \theta_c}{\sqrt{M_\infty^2 - 1}} \qquad (1)$$

where θ_c = cone half-angle.

The base drag at subsonic speeds is

$$C_{D_B} = \frac{0.029}{C_{D_{ZL}}} \qquad (2)$$

where

C_{D_B} = base drag coefficient

$C_{D_{ZL}}$ = zero lift drag coefficient

from Fig. 37, pages 3 to 19 of Ref. 3. Above $M_\infty = 1.0$ the base drag of a cylindrical forebody is presented in Ref. 4. Reference 5 relates the base drag with flared forebody to cylindrical forebody. Total aerodynamic drag is presented in Fig. 2 as a function of Mach number.

Corrections for viscous effects at hypersonic speeds were calculated using the following method.

Cone friction drag is

$$C_{D_f} = \frac{A\,\overline{C}_f}{A_{ref}} \cos\theta_c \qquad (3)$$

where A is cone surface area and $\overline{C}_f$ is average cone friction coefficient

$$\overline{C}_f = \frac{\int_A C_f \, dA}{\int_A dA} \qquad (4)$$

From Ref. 6 the friction coefficient for a flat plate is:

$$C_f = \frac{0.664}{\sqrt{Re_s}} \left(\frac{V_2}{V_\infty}\right)^{3/2} \left(\frac{p_2}{p_\infty}\right)^{1/2} \left[\left(\frac{1}{2} - 0.22\,\overline{r}\right)\frac{i_2}{i_\infty} + \frac{i_w}{2i_\infty} + 0.22\,\overline{r}\left(1 + \frac{(\overline{\gamma}_\infty - 1)\,M_\infty^2}{2}\right)\right]^{-0.191} \qquad (5)$$

where $\overline{r}$ is the recovery factor, $\sqrt{0.71}$, and Re_s is the local Reynolds number.

For a cone, V_2, p_2, and i_2 are velocity, pressure and enthalpy at the boundary layer edge and are, in the Newtonian approximation, given by

$$\left.\begin{aligned}
\frac{V_2}{V_\infty} &= 1 - B \sin^2 \theta_c \\
\frac{p_2}{p_\infty} &= B\bar{\gamma}_\infty M_\infty^2 \sin^2 \theta_c \\
\frac{i_2}{i} &= \frac{\bar{\gamma}_\infty - 1}{2} B M_\infty^2 \sin^2 \theta_c
\end{aligned}\right\} \tag{6}$$

The local friction coefficient for a flat plate

$$C_{f_c} = 1.47 \frac{M_\infty^{0.618}}{\sqrt{Re_\ell}} B^{1/2} \sin \theta_c \left(1 - B \sin^2 \theta_c\right)^{3/4} \left(\frac{\ell}{s}\right)^{1/2} =$$

$$\frac{K}{s^{1/2}} \tag{7}$$

where Re_ℓ is Reynolds number based on vehicle length and freestream conditions.

θ_c = cone half-angle

B = a constant (1.12) that relates test pressures to Newtonian theory values

s = streamline distance from nose of cone

ℓ = the cone length

$$A\bar{C}_f = \int_0^s \frac{K2 \pi r\, ds}{s^{1/2}} = \frac{4}{3} \pi \sin \theta_c \frac{K\ell^{3/2}}{\cos^{3/2} \theta_c} \tag{8}$$

and cone surface area,

$$A = \frac{\pi r_B \ell}{\cos \theta_c} \quad \text{where } r_B \text{ is the radius of the cone base}$$

$$C_{D_f} = \sqrt{3} \frac{\cos \theta_c}{A_B} \frac{4}{3} \pi \sin \theta_c \frac{\ell^{3/2}}{\cos^{3/2} \theta_c} \left[1.47 \frac{M_\infty^{0.618}}{\sqrt{Re_\ell}} B^{1/2} \sin \theta_c\right.$$

$$\left(1 - B \sin^2 \theta_c\right)^{3/4} \ell^{1/2} \Bigg] \qquad (9)$$

where

$\ell = 2.33$ ft (0.71 m)

$\theta_c = 25°$

$A_B = 4.92\ \text{ft}^2\ (0.457\ \text{m}^2)$ base area of cone

$\sqrt{3}$ = the Mangler transformation constant going from flat plate to cone

$$\frac{C_{D_f}}{M_\infty^{0.618} / \sqrt{Re_\ell}} = 2.19 \qquad (10)$$

Presentation of Trajectory Results

The axisymmetric re-entry trajectory parameters are presented in Figs. 3 and 4 as a function of time from re-entry altitude. Maximum axial load factor reached 11.21 g at 118,262 ft (36,100 m) at a relative velocity of 12,517 ft/sec (3.815 km/s). Maximum dynamic pressure of 1081.15 psf (51,766 N/m^2) occurred 185 sec after re-entry at an altitude of 124,166 ft (37,850 m) and a relative velocity of 14,311 ft/sec (4.362 km/s). Touchdown occurred 358 sec after re-entry, and 800 n. mi. (1.482 mm) downrange at Mach 0.396.

HEAT RATE, SHEAR STRESS AND FLOW FIELD

The axisymmetric vehicle (Fig. 1) is a 25° half-angle cone with a 3-in. radius spherically blunted nose and a 30-in. diameter base. No experimental heat transfer or pressure data were found for this particular vehicle configuration. Pressure data from Ref. 7, which presents method-of-characteristics solutions for blunted cone pressure distributions at hypersonic speeds (M = 10 data used) have been checked against available experimental data for 20° and 30° cones and found to correlate extremely well. The pressure distribution used in the present study is shown in Fig. 5. This pressure distribution was used in the FB047 digital computer program (see Ref. 1) to derive the laminar heat transfer rate distributions shown in Fig. 6. Data for 10 different times (t = 50, 80, 100, 130, 155, 180, 190, 205, 220 and 230 sec) in the re-entry trajectory for the axisymmetric vehicle were calculated.

Theory:

The theoretical analysis of the laminar and turbulent heat transfer rates, shear stresses at the wall and local flow properties external to the boundary layer for this study have been calculated by an IBM 7094 digital computer program: FB047. This program considers blunt bodies in axisymmetric or two-dimensional flow and, therefore, is directly applicable to the analysis of the axisymmetric vehicle. The theoretical analytical methods incorporated in FB047 are summarized here:

1. Laminar boundary layer. --The laminar heat transfer rate distribution utilizes the method of Eckert and Tewfik (Ref. 8). The basic $\dot{q}$ (laminar) distribution equation is

$$\frac{\dot{q}_s}{\dot{q}_0} = \left[\frac{k_s^*}{k_0^*}\right]\left[\frac{H_s^*}{H_0^*}\right]\left[\frac{i_{rec} - i_w}{i_0 - i_w}\right]\left[\frac{C_{p_{w_o}}}{C_{p_{w_s}}}\right] \qquad (11)$$

in which the starred quantities are evaluated at local (s) pressure and the local reference enthalpy. The reference enthalpy is defined as

$$i_{ref} = i_s^* = \frac{i_s + i_w}{2} + 0.22\sqrt{Pr_s}\,(i_0 - i_s) \qquad (12)$$

The recovery enthalpy i_{rec} (see Eq. 1) is derived from

$$\begin{aligned} &\text{Laminar} && i_{rec} = i_s\left(1 - \sqrt{Pr_s^*}\right) + i_0\sqrt{Pr_s^*} \\ &\text{Turbulent} && i_{rec} = i_s\left(1 - \sqrt[3]{Pr_s^*}\right) + i_0\sqrt[3]{Pr_s^*} \end{aligned} \qquad (13)$$

in which the total enthalpy, i_0, is

$$i_0 = i_\infty + V_\infty^2 \qquad (14)$$

The functions H_s^* and H_0^* are defined as

$$H_s^* = \frac{\left[p_s^*/\rho_0\right]\left[V_s/V_\infty\right]\left[r_s\right]^Z}{\left[\int_0^s \left(\frac{\rho_s^*}{\rho_0}\frac{\mu_s^*}{\mu_0}\right)\left(\frac{V_s}{V_\infty}\right)(r_s)^{2Z}\,ds\right]^{1/2}} \qquad (15)$$

and

$$H_0^* = \left[\frac{2\,(\rho_0^*/\rho_0)\,(dV/ds)_0}{V_\infty\,(\mu_0^*/\mu_0)} \right]^{1/2} (1 + Z)^{1/2} \tag{16}$$

where in Eqs. 15 and 16

$Z = 0$ for 2-dimensional flow

$Z = 1$ for axisymmetric flow

The Newtonian stagnation point velocity gradient is used in Eq. 16.

$$\left(\frac{dV}{ds}\right)_0 = \frac{\sqrt{2}}{R_N} \left[\frac{p_0 - p_\infty}{\rho_0}\right]^{1/2} \tag{17}$$

The required input for each problem includes the nose radius, R_N, the altitude, free stream velocity, a listing of s stations (s = surface distance along a streamline from the stagnation point to the point being investigated), $r = f(s)$ (normal distance from the free stream velocity vector which passes through the stagnation point to the body surface point--sometimes called local flow displacement distance), $p = f(s)$ the pressure distribution, ρ_∞/ρ_0, the density ratio across a normal shock at the appropriate free stream velocity and altitude, and $T_{wall} = f(s)$. With this input data, the program employs a subroutine of Hansen's Mollier and transport data (Ref. 9) using constant total enthalpy and constant entropy to obtain the local external-to-boundary-layer (s), wall (w) and reference (in the boundary layer, *) flow conditions: ρ, μ, k, C_p, h, etc.

The local velocity external to the boundary layer is obtained from the energy equation

$$\frac{V_s}{V_\infty} = \frac{224\,(i_0 - i_s)^{1/2}}{V_\infty} \tag{18}$$

The shear stress and friction coefficient calculations for both laminar and turbulent boundary layers are derived directly from the calculated heat transfer rate, local flow properties and Reynold's Analogy

$$C_f = \frac{2\,\dot{q}_s\,(Pr_s^*)^{2/3}}{\rho_s\,V_s\,(i_{rec} - i_w)\,g} \tag{19}$$

$$\tau = 0.5\,C_f\,\rho_s\,V_s^2 \tag{20}$$

if the laminar value for $\dot{q}$ is used in Eq. 19, C_f and τ will be the laminar values; similarly, turbulent $\dot{q}$ in Eq. 19 yields the turbulent friction coefficient--thence (Eq. 20) the turbulent wall shear stress.

Note that Eqs. 11, 15 and 16 are used only to obtain the laminar heat transfer rate distribution.

2. Stagnation point. --The stagnation point heat transfer rate is calculated by the Fay and Riddell equation (Ref. 10).

$$\dot{q}_0 = 0.76\,(Pr)^{-0.6}(\rho_w\mu_w)^{0.1}\;(\rho_s\mu_s)^{0.4}\;(i_0 - i_w)\left(\frac{dV}{ds}\right)_0^{1/2} g \tag{21}$$

(Lewis No. assumed = 1.0)

3. Turbulent boundary layer. --The turbulent heat transfer rate is calculated by means of the turbulent "Flat Plate Reference Enthalpy" equation, as shown on p 21 of Ref. 11, which is transformed to the form

$$\dot{q}_{turb} = 0.03\,g^{1/3}\,(1+Z)^{0.2}\left(k_s^*\right)^{2/3}\left(\rho_s V_s\right)^{0.8}$$

$$\left[\left(1 - \left\{Pr_s\right\}^{1/3}\right) i_s + (Pr_s)^{1/3}\,i_0 - i_w\right]\left[\left(\mu_s^*\right)^{7/15}$$

$$\left(C_{p_0}^*\right)^{2/3}(s)^{0.2}\right]^{-1} \tag{22}$$

The local Reynolds number is

$$Re_s = \frac{\rho_s V_s s}{\mu_s} \tag{23}$$

Note that the first term in brackets in Eq. 22 is merely $(i_{rec} - i_w)$ for the turbulent boundary layer.

The foregoing discussion describes only those features of FB047 which have been used in this study. Caution must be used in the interpretation of the turbulent shear stresses and heat rates calculated by FB047. They are valid only when greater than the calculated laminar values.

Presentation of Data:

In order to evaluate the effects of heating distribution changes with velocity and altitude, a weighted mean value of $\dot{q}_s/\dot{q}_0$ was calculated in the following manner:

$$\phi_t = \frac{\dot{q}_s}{\dot{q}_0} \text{ at time t}$$

$$X_t = \frac{\dot{q}_0 \text{ at time t}}{\dot{q}_0 \text{ max in re-entry}} \qquad (24)$$

then

$$\left[\frac{\dot{q}_s}{\dot{q}_0}\right]_{\text{weighted mean}} = \frac{\sum\limits_t \phi_t X_t}{\sum\limits_t X_t} \qquad (25)$$

The maximum difference between $\dot{q}_s/\dot{q}_0$ evaluated at the time of $\dot{q}_{0_{max}}$ in the trajectory and the weighted mean value was found to be less than 1.7%. Since the weighted mean values are more meaningful in a heat shield design, these values are plotted in Fig. 6. In any case, the two distributions are so close as to appear virtually identical on the plot. Note that all $\dot{q}$ and τ calculations are based upon $T_w = 540°$ R (300° K).

The stagnation point time histories of heat transfer rate, density, viscosity, pressure, temperature and enthalpy are shown in Figs. 7, 8 and 9. Note that the time is given in seconds from the initiation of re-entry called out in the specified initiating conditions (433,200-ft altitude).

Figures 10 through 20 present the laminar and turbulent heat rates and shear stresses at the wall, local Mach number, viscosity, temperature, enthalpy, pressure, density and Reynolds number based on local flow properties and surface distance from the stagnation point $\left(Re_s\right)$. These functions are given for s/R_N

stations 1.0, 2.25, 3.0, 4.0, 5.0 and 10.0 where s is the surface distance from the stagnation point and R_N is the nose radius. The turbulent heating and shear stress data are valid only when greater than the corresponding laminar value. The sonic point occurs at approximately $s/R_N = 0.7$.

Figure 20 shows that for the specified re-entry trajectory and with a local transition Reynolds number (Re_s) assumed to be 10^6, there is virtually no turbulent flow anywhere on the vehicle during the significant heating portion of the re-entry trajectory.

Attention is called to the fact that no really satisfactory theoretical method of predicting transition from laminar to turbulent flow is presently available. A set of criteria currently used by the Martin Company conservatively assumes a transition momentum thickness Reynolds number of 200 for the subsonic local flow portion of the flow field and a transition local Reynolds number (based on streamline distance from the stagnation point) of 1×10^6 for the supersonic local flow regions. The conservatism of these criteria is adequately documented by both wind tunnel and free flight experiments as reported in Refs. 12 to 15. The axisymmetric vehicle momentum thickness Reynolds number in the nose region never reaches 200 and the local Reynolds number back on the body never reaches 1×10^6 so no transition is indicated.

CONCLUDING REMARKS

A re-entry trajectory for a 25° half-angle, spherically blunted conical vehicle has been generated for a ballistic re-entry (angle of attack = 0 deg). Calculated data presented in this report include the variation of vehicle drag coefficient with free-stream Mach number, histories through re-entry of range, stagnation point heat transfer rate and total heat, resultant load factor, free-stream Reynolds number (based on vehicle length), altitude, relative velocity, free-stream Mach number and dynamic pressure. In addition, pressure and heat transfer rate distributions over the vehicle are included along with histories through re-entry of stagnation point density, pressure, viscosity, temperature and enthalpy. Local laminar and turbulent histories of heat transfer rates and wall shear stresses are given for vehicle stations: s/R_N (surface distance from stagnation point non-dimensionalized with nose radius) = 1.0, 2.25, 3.0, 4.0, 5.0 and 10.0. Local (external-to-boundary layer) histories of pressure, density, Mach number, enthalpy, viscosity, temperature and Reynolds number are presented for the same body stations.

If a value of local Reynolds number of one million is assumed to define transition from laminar to turbulent flow, the subject vehicle will experience no turbulent heating during the significant heating portion of re-entry.

Martin Company
Baltimore, Maryland 21203
March 28, 1966

REFERENCES

1. Wing, L. D.; and Eilertson, W. H.: Research Studies and Analysis to Define Manned Lifting Entry Flight Environment. NASA CR 307E (C), January 1966.

2. Wagner, W. E.; and Garner, W. R., Jr.: Near Earth Flight Analysis Program (UB088) Summary Report. ER 13465, Martin Marietta Corporation, Baltimore, Md., June 1964. (U).

3. Hoerner, S. F.: Fluid Dynamic Drag. Library of Congress Catalog No. 57-13009, 1958. (U).

4. Love, E. S.: The Base Pressure at Supersonic Speeds on Two-Dimensional Airfoils and Bodies of Revolution Having Turbulent Boundary Layers. NACA TN 3819, January 1957. (U).

5. Wakefield, R. M.; Knechtel, E. D.; and Treon, S. L.: Transonic Static Aerodynamic Characteristics of a Blunt Cone-Cylinder Body with Flared Afterbodies of Various Angles and Base Areas. NASA TMX-106, December 1959. (No classified data from this reference is given or recorded in Vol. II.)

6. Maslen, S.: Considerations in the Design of Vehicles Capable of Substantial Hypersonic Lift Drag Ratios. Research Report RR-54, Martin Marietta Corporation, Baltimore, Md., March 1964. (U).

7. Chushkin, P. I.; and Shulishnina, N. P.: (Academy of Sciences USSR, Moscow): Tables of Supersonic Flow About Blunted Cones. Technical Memo RHD-TM-62-63, AD No. 287187 (Translated by J. F. Springfield), Research and Advanced Development Division, AVCO Corp., Wilmington, Mass., September 14, 1962.

8. Eckert, E. R. G.; and Tewfik, O. E.: Use of Reference Enthalpy in Specifying the Laminar Heat Transfer Distribution Around Blunt Bodies in Dissociated Air. (U). Journal of the Aero/Space Sciences Vol. 27, No. 6, June 1960, p 464.

9. Hansen, C. F.: Approximations for the Thermodynamic and Transport Properties of High Temperature Air. (U). NASA TR R-50, 1959.

10. Fay, J. A.; and Riddell, F. R.: Theory of Stagnation Point Heat Transfer in Dissociated Air. (U). Journal of the Aero/Space Sciences, Vol. 25, No. 2, February 1958, p 73.

11. Libby, P. A.; and Cresci, R. J.: Evaluation of Several Hypersonic Turbulent Heat Transfer Analyses by Comparison with Experimental Data. (U). WADC Tech. Note 57-72, ASTIA Doc. No. AD 118093, July 1957.

12. Allen, H. J.; Seiff, A.; and Winovich, W.: Aerodynamic Heating of Conical Entry Vehicles at Speeds in Excess of Earth Parabolic Speed. NASA TR R-185, December 1963. (U).

13. Sternberg, J.: A Free-Flight Investigation of the Possibility of High Reynolds Number Supersonic Laminar Boundary Layers. Journal of the Aeronautical Sciences, pp 721-733, Vol. II, November 1952. (U).

14. Tetervin, N.: Comparison of Transition Location on Blunt Bodies in Supersonic Flight with Calculated Laminar Boundary Layer Stability Position and Calculated Most Forward Possible Transition Position. Pre-print from paper delivered at 5th U. S. Navy Symposium on Aeroballistics at U. S. Naval Ordnance Laboratory, White Oak, Md. October 1961. (U).

15. Deem, R. E.; and Murphy, J. S.: Flat Plate Boundary Layer Transition at Hypersonic Speeds. AIAA Paper No. 65-128. AIAA 2nd Aerospace Sciences Meeting, New York City. January 1965. (U).

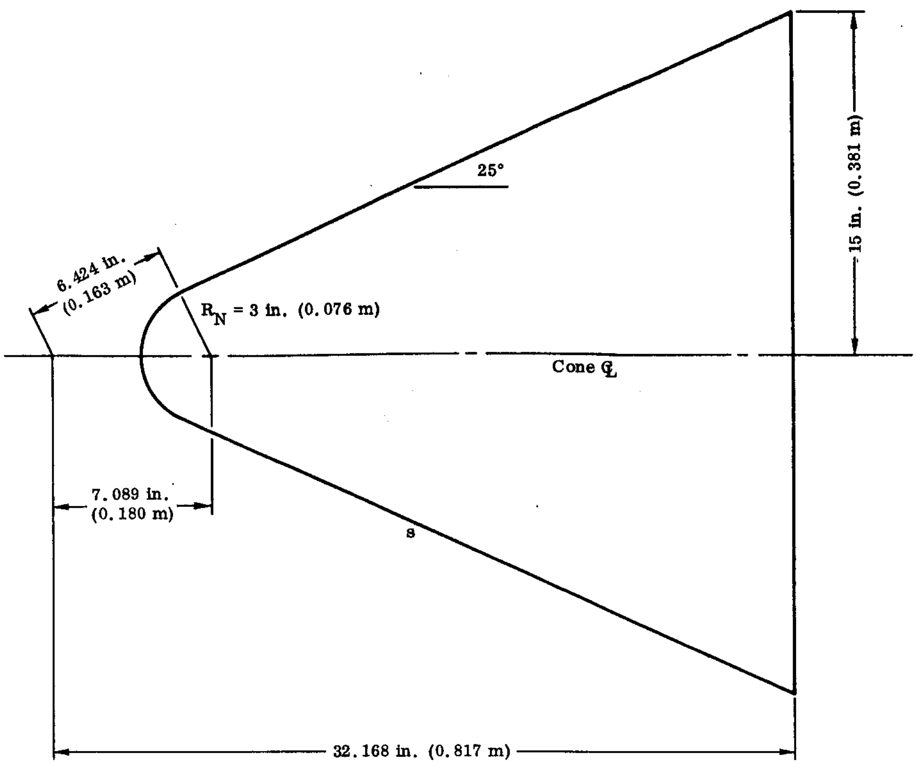

Fig. 1. Sketch of the Axisymmetric Vehicle

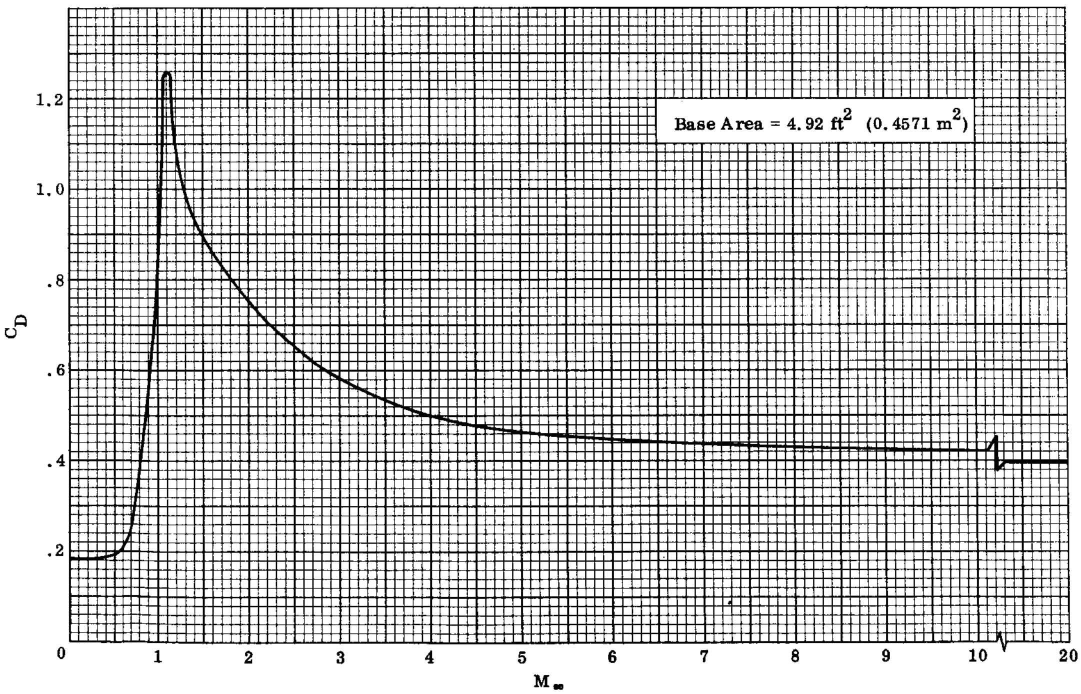

Fig. 2. Axisymmetric Configuration Inviscid Drag Coefficient

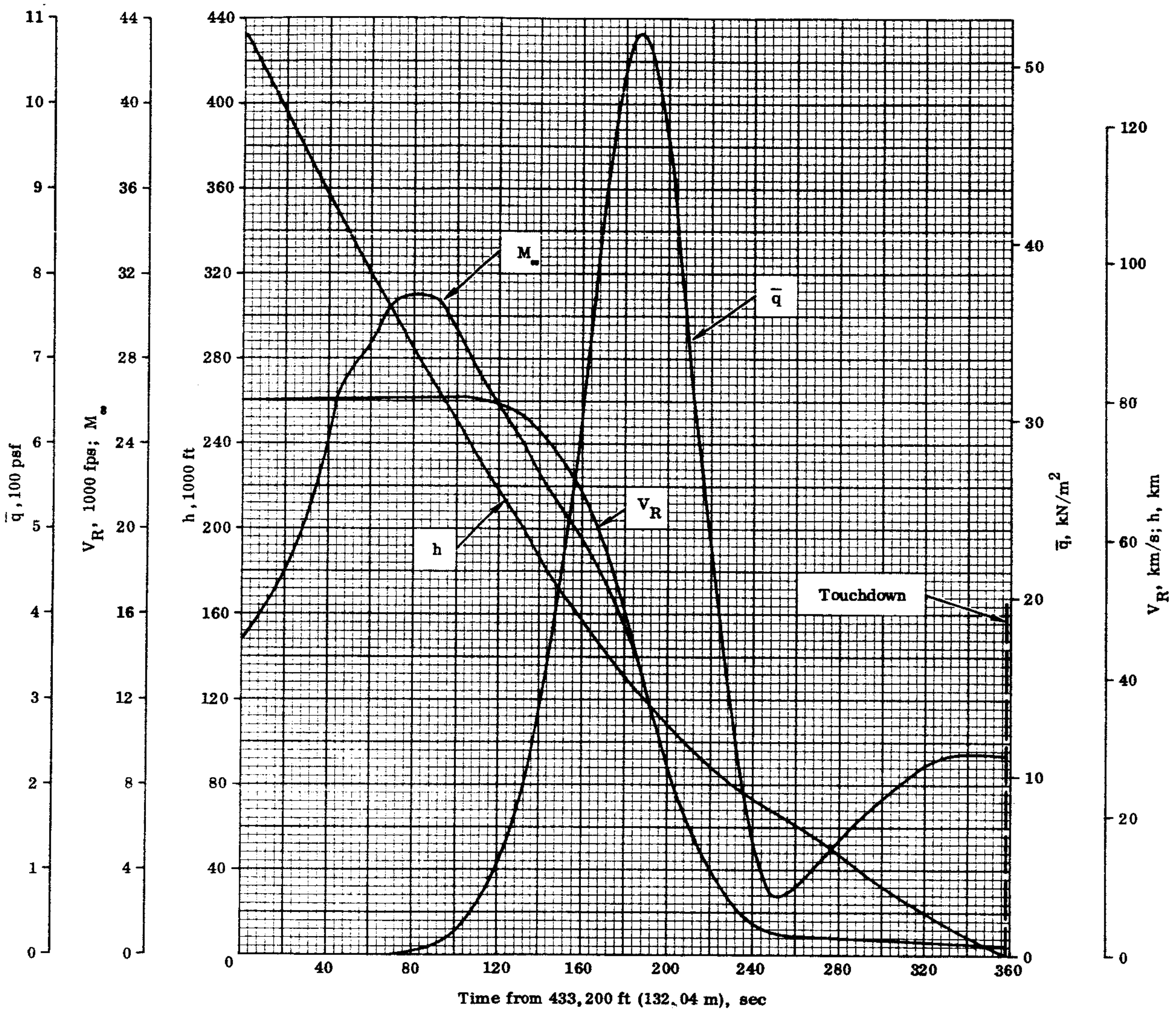

Fig. 3. Axisymmetric Configuration Re-entry Trajectory

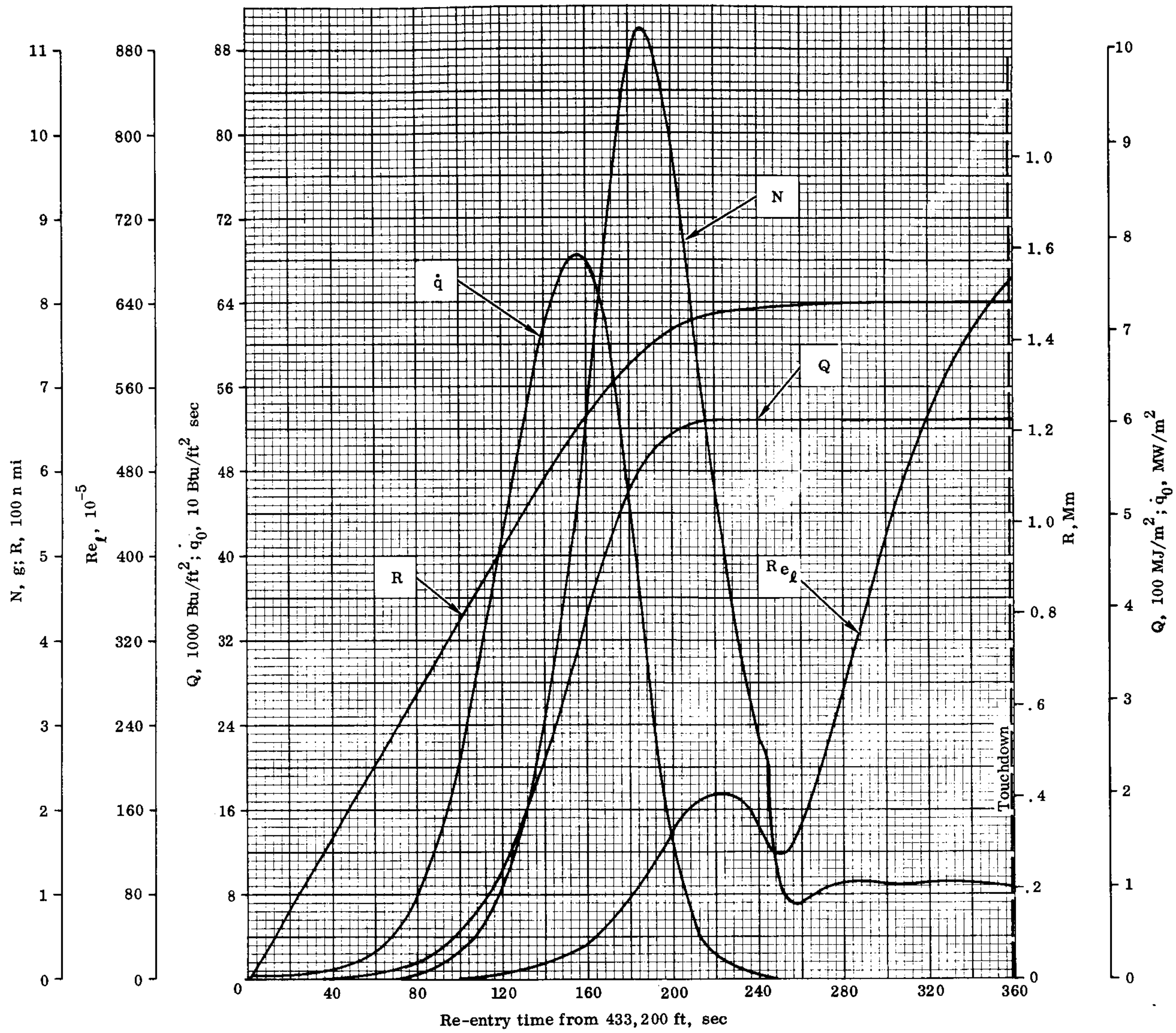

Fig. 4. Axisymmetric Configuration Re-entry Trajectory

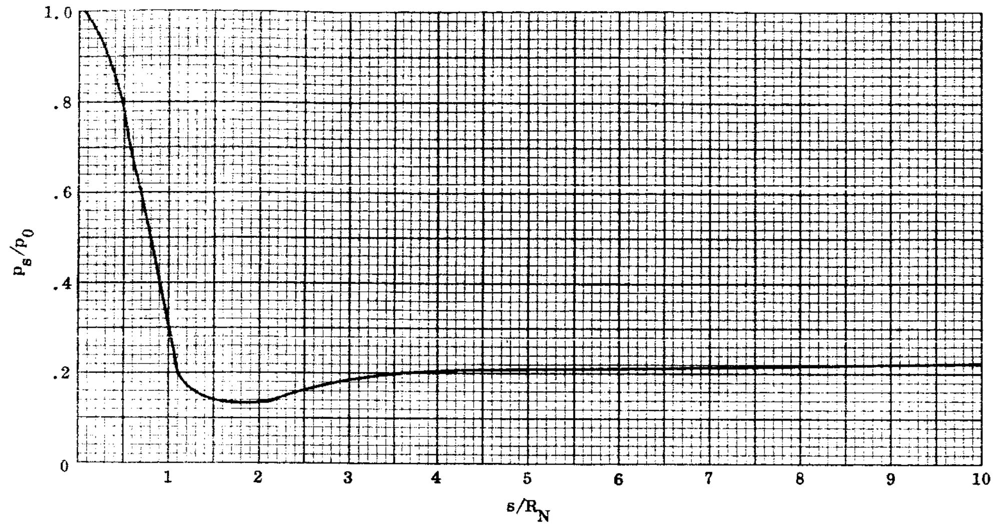

Fig. 5. Pressure Distribution on Axisymmetric Vehicle, $\alpha = 0°$

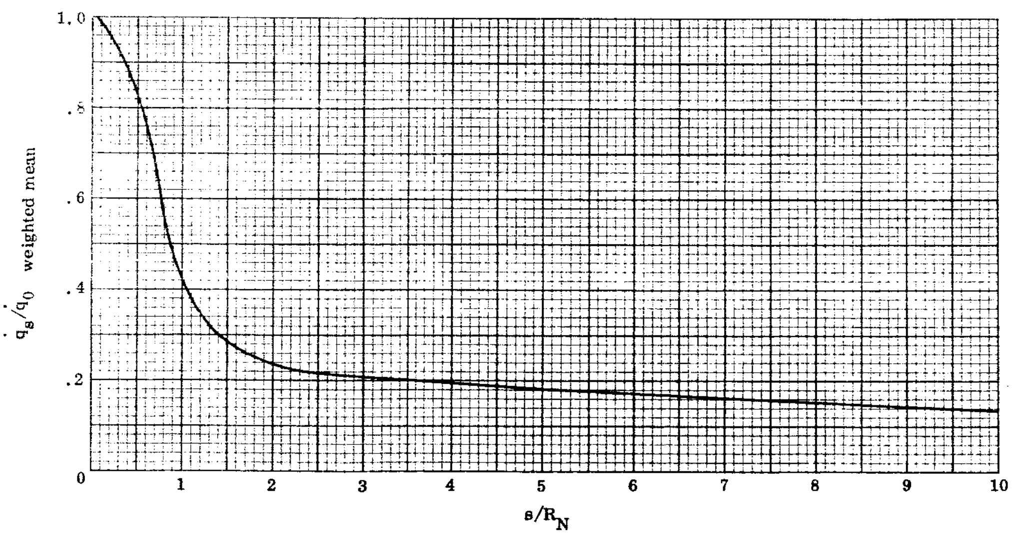

Fig. 6. Weighted Mean Heat Rate Distribution Over Ten Times in the Re-entry Trajectory, Laminar Flow; $\alpha = 0°$

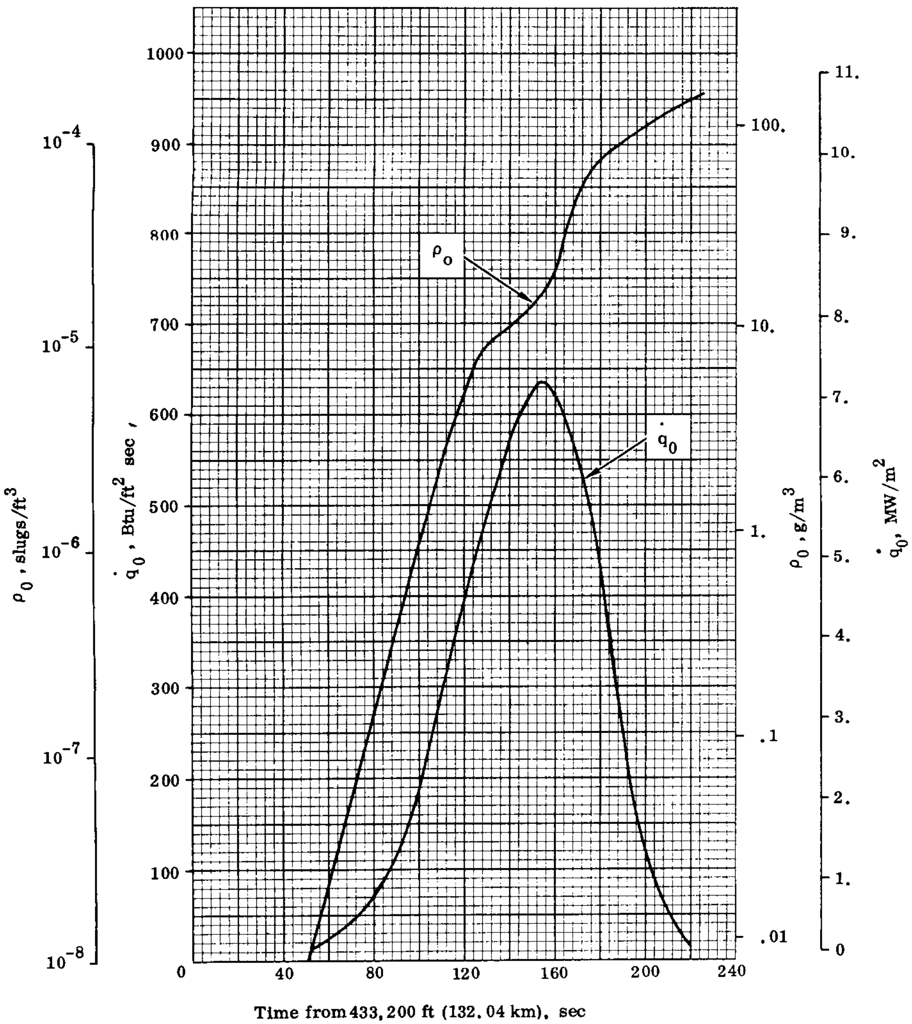

Fig. 7. Stagnation Point Heat Rate and Density Histories

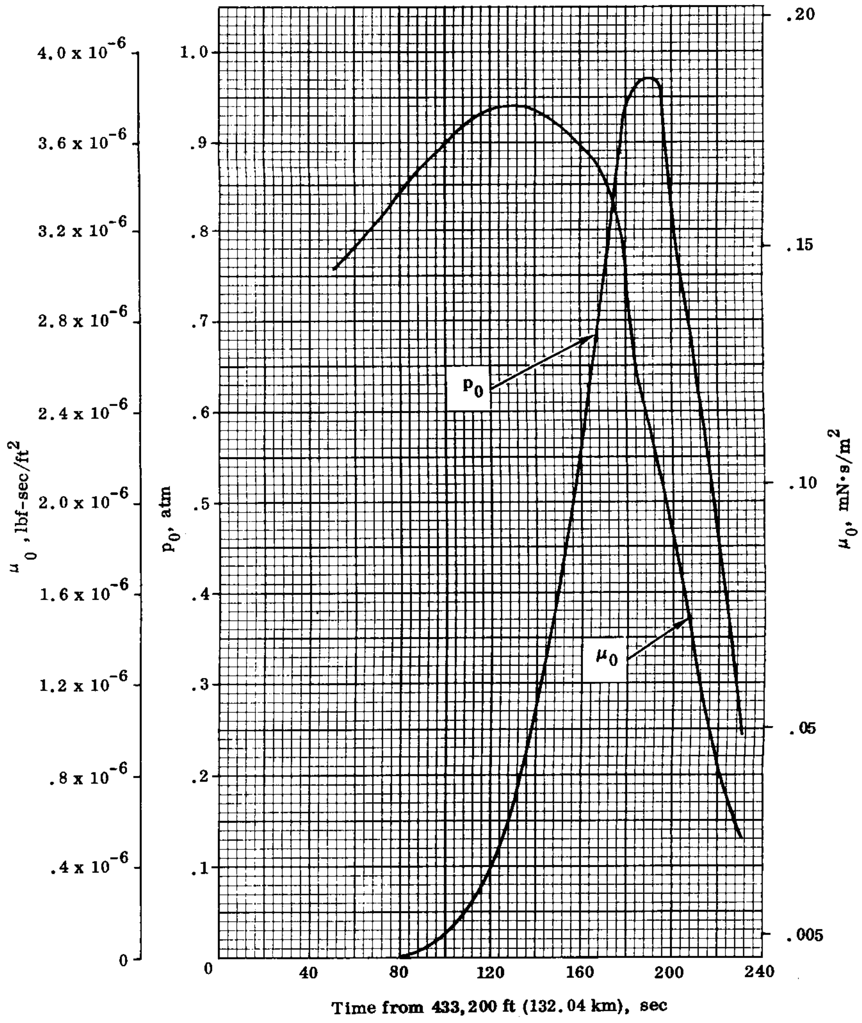

Fig. 8. Stagnation Point Pressure and Viscosity Histories

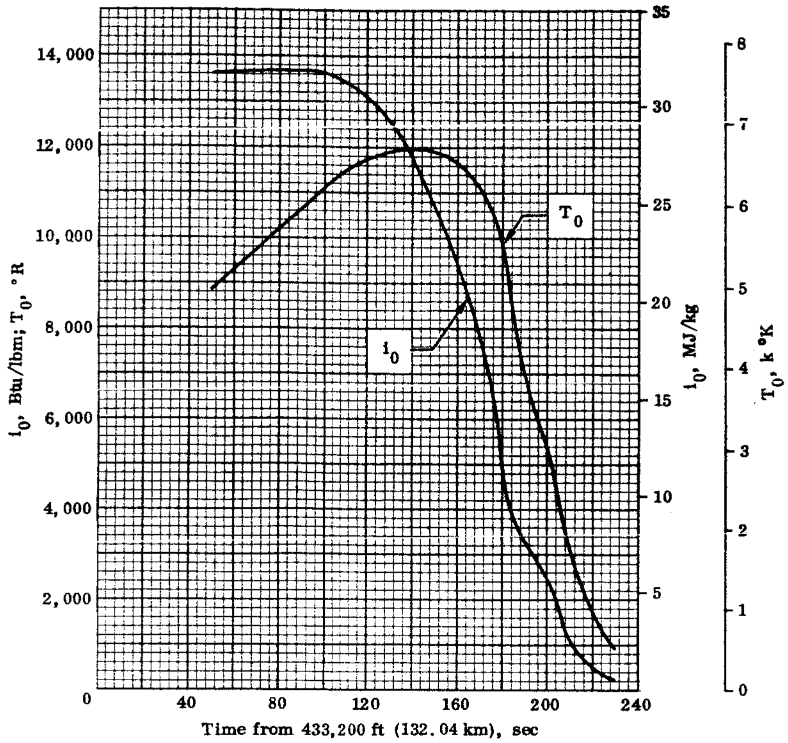

Fig. 9. Stagnation Point Temperature and Enthalpy Histories

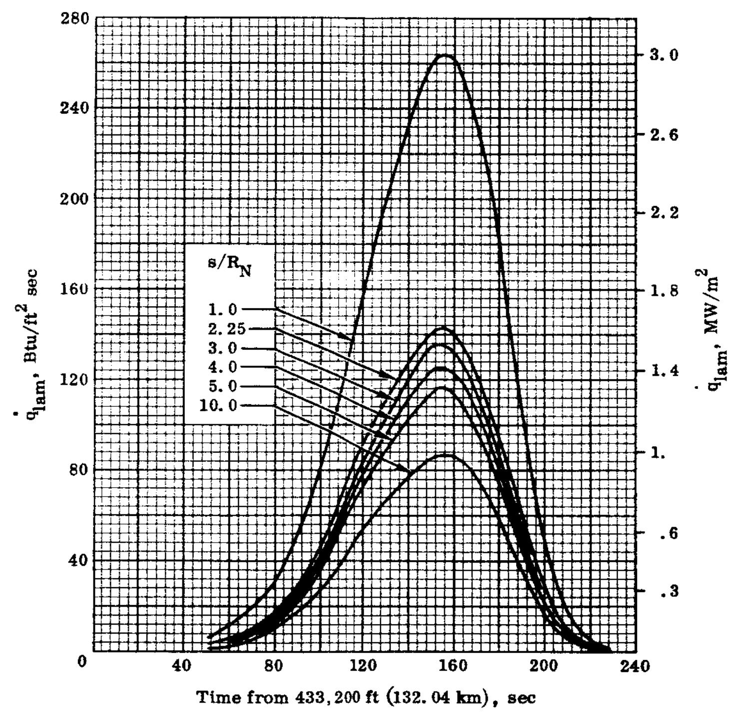

Fig. 10. Laminar Heat Rate Histories for Several s/R_N Stations

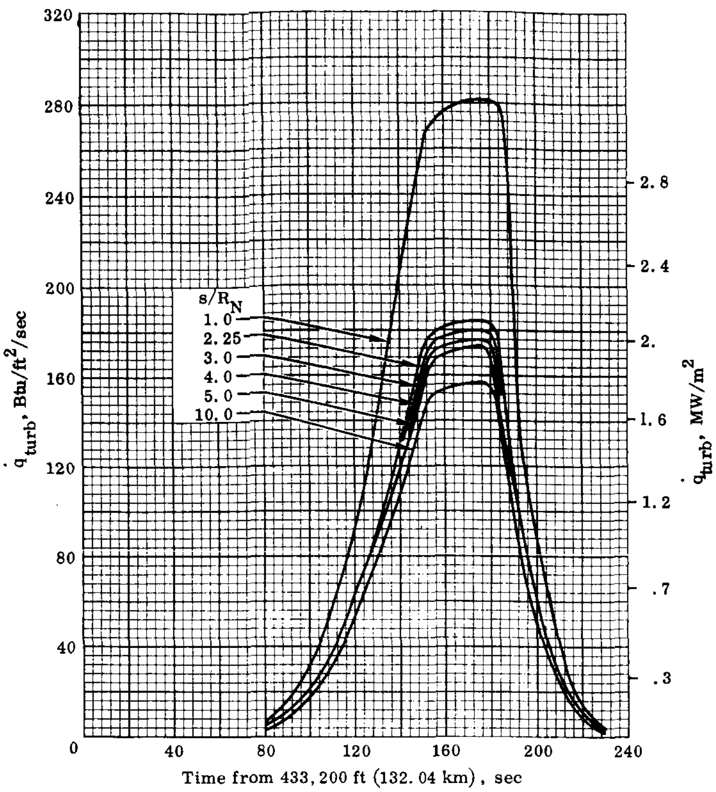

Fig. 11. Turbulent Heat Rate Histories for Several s/R_N Stations (applicable only when greater than laminar value)

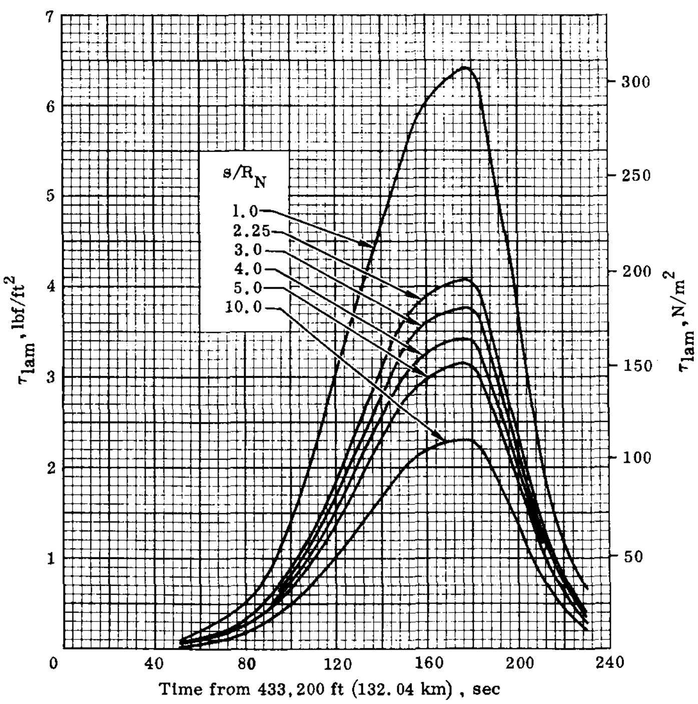

Fig. 12. Laminar Shear Stress at Wall Histories for Several s/R_N Stations

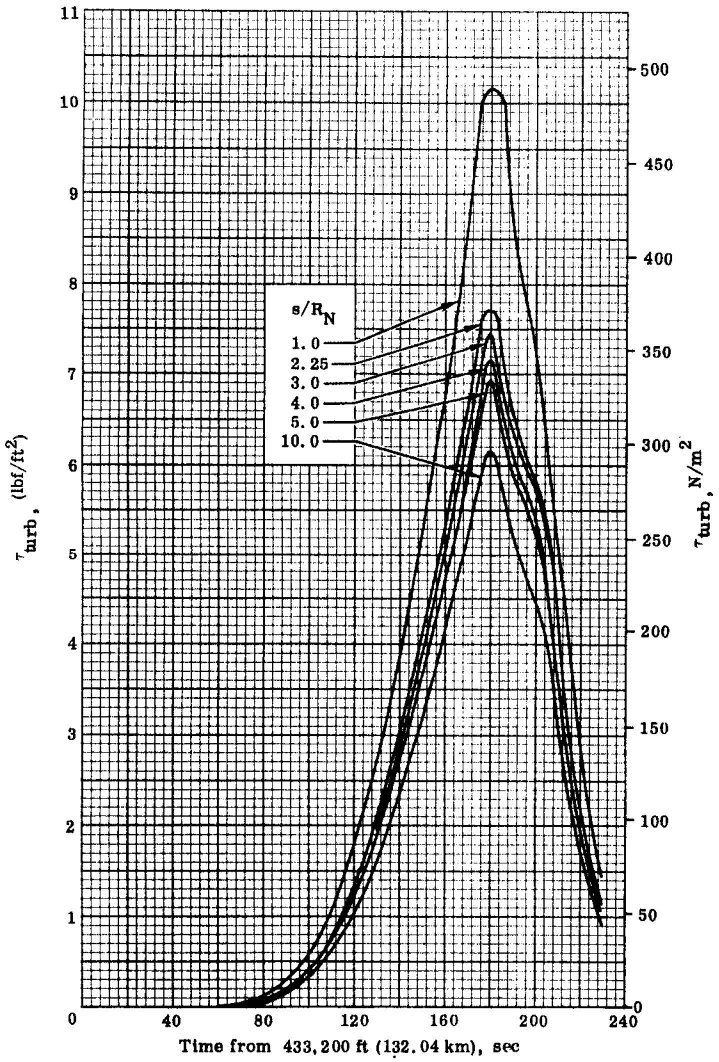

Fig. 13. Turbulent Shear Stress at Wall Histories for Several s/R_N Stations (applicable only when greater than laminar value)

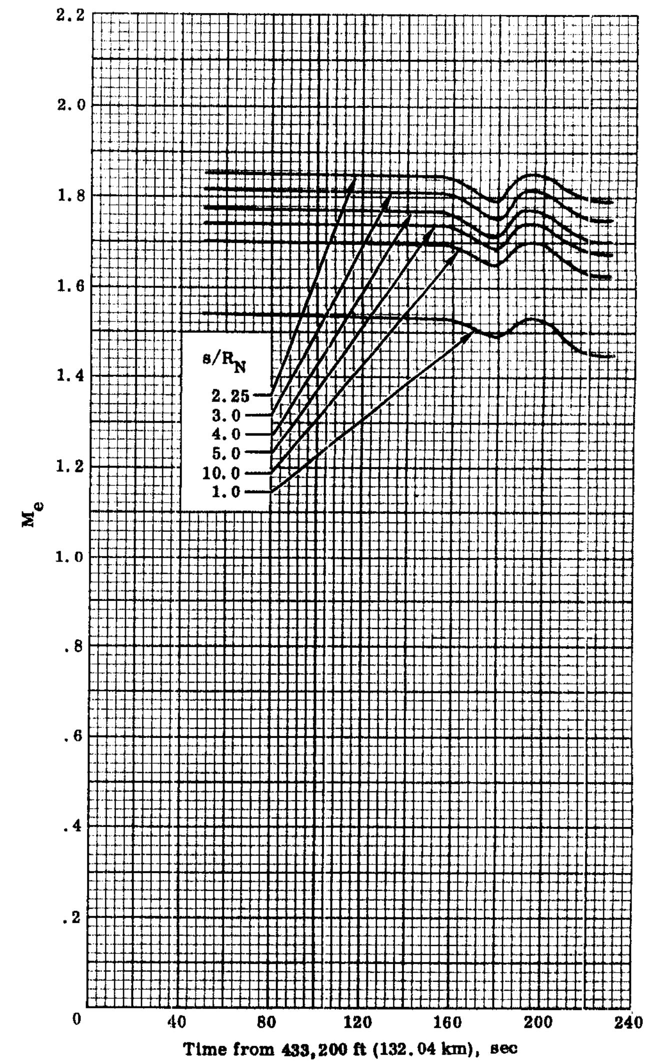

Fig. 14. Local Mach Number Histories for Several s/R_N Stations

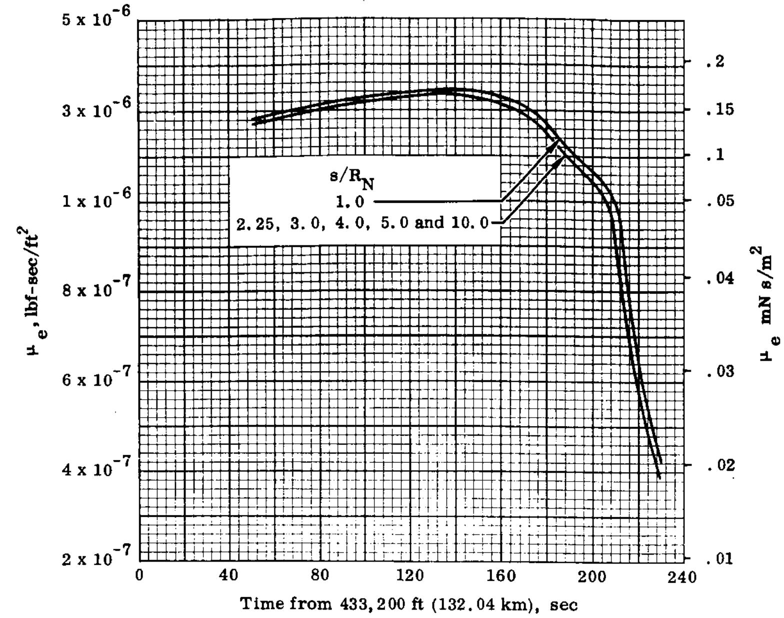

Fig. 15. Local Viscosity Histories for Several s/R_N Stations

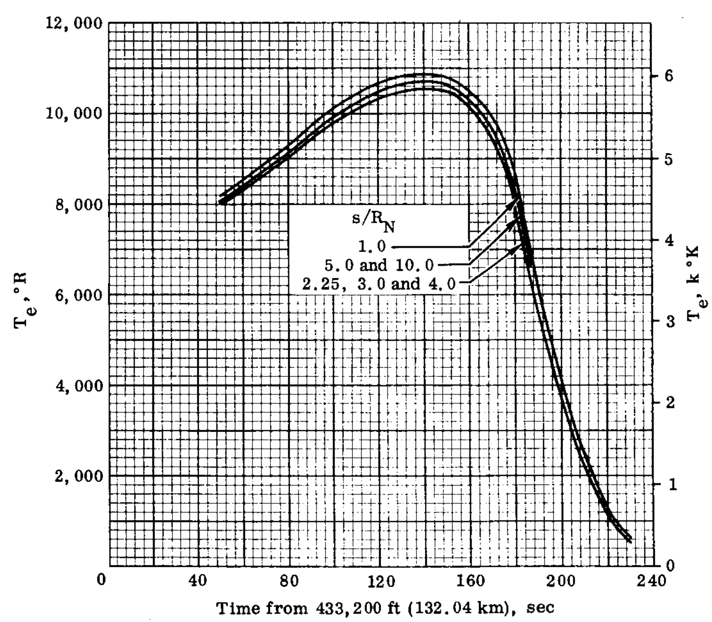

Fig. 16. Local Temperature Histories for Several s/R_N Stations

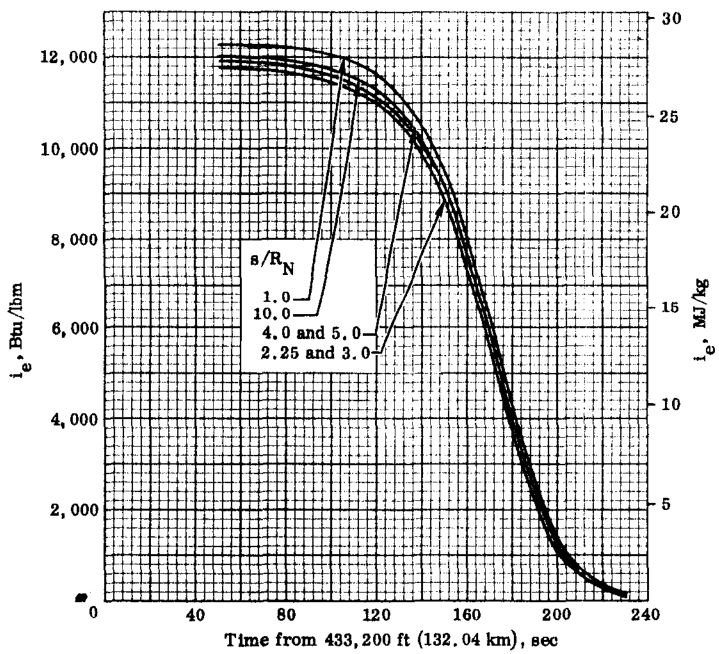

Fig. 17. Local Enthalpy Histories for Several s/R_N Stations

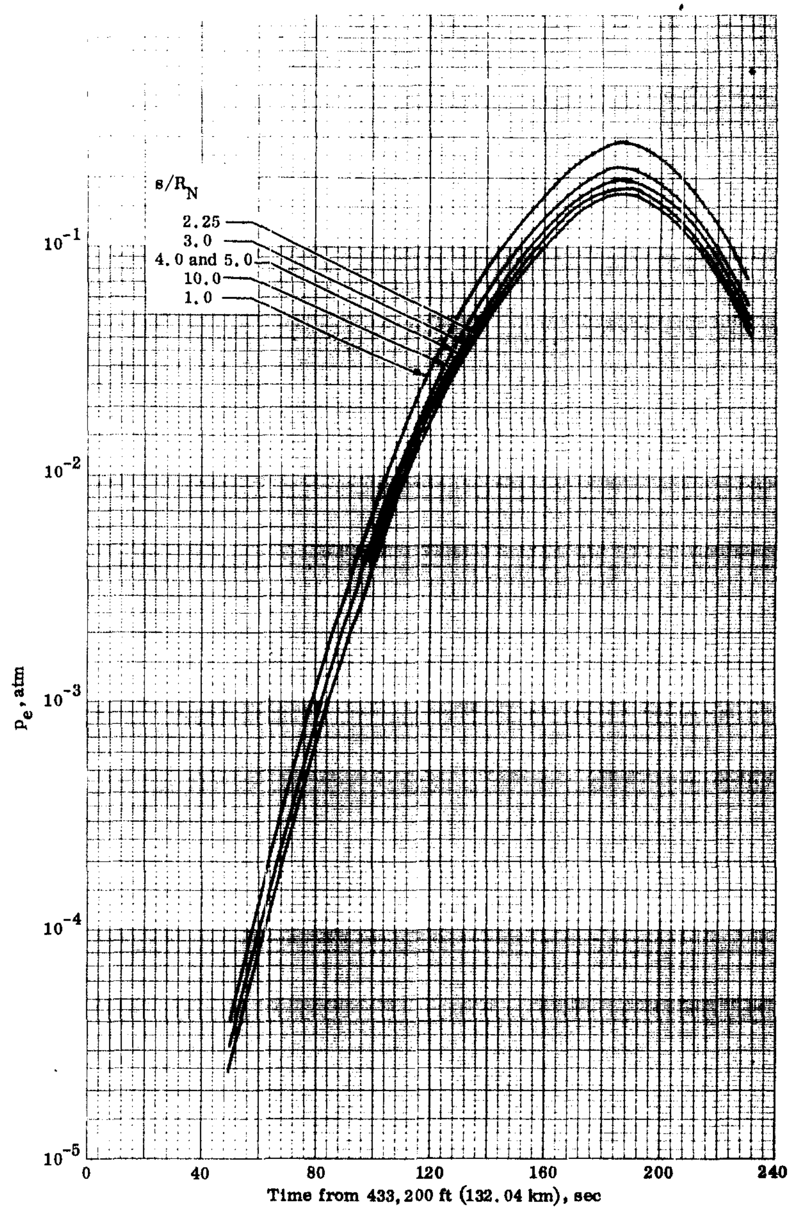

Fig. 18. Local Pressure Histories for Several s/R_N Stations

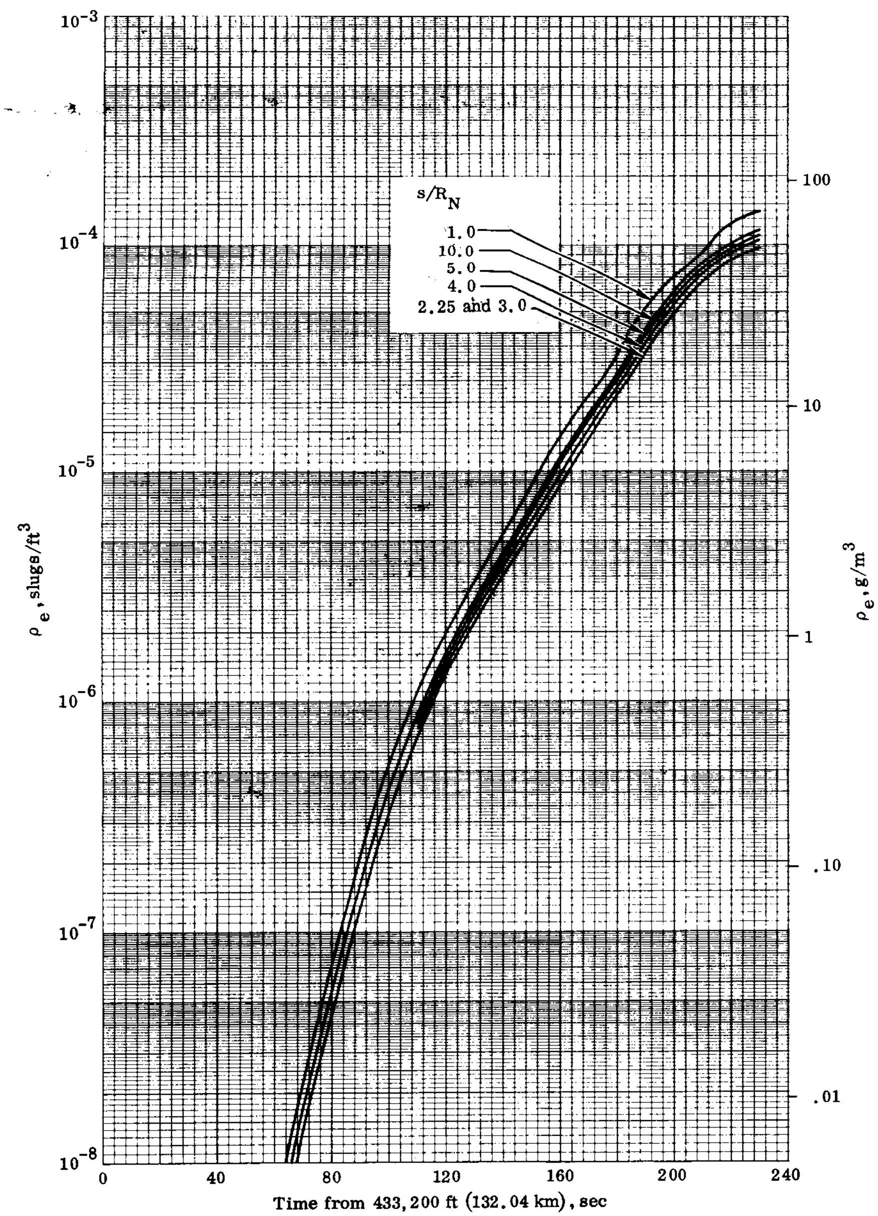

Fig. 19. Local Density Time Histories for Several s/R_N Stations

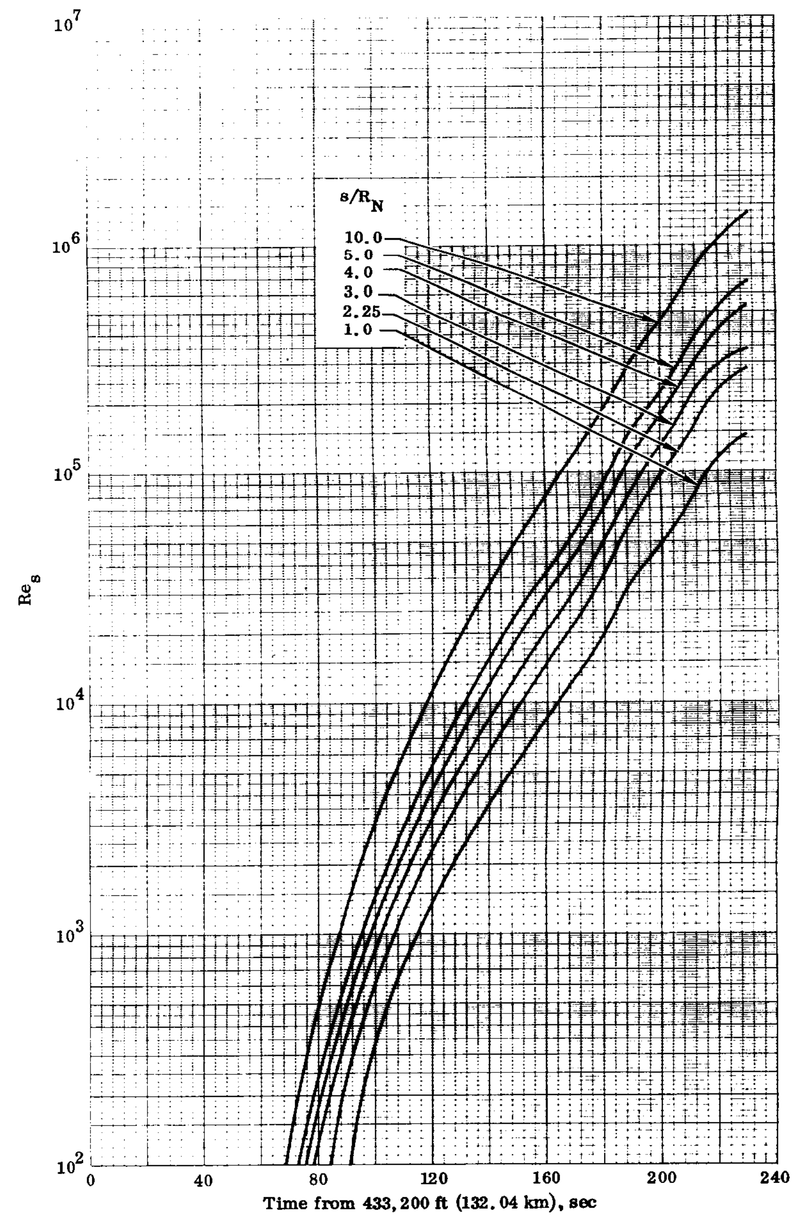

Fig. 20. Local Reynolds Number Time Histories for Several s/R_N Stations